 https://doi.org/10.3311/PPee.40008

Periodica Polytechnica Electrical Engineering and Computer Science, 69(4), pp. 372–378, 2025

Modeling and Detecting the Demagnetization Fault in the Permanent Magnet Synchronous Machine Using the Current Signature Analysis

Nadia Radja[1*], Nacera Yassa[2], M'hemed Rachek[1], Hamza Houassine[2]

[1] Department of Electrical Engineering, University of Mouloud Mammeri Tizi-Ouzou, Nouvelle ville 17 RP, 15000 Tizi Ouzou, Algeria
[2] Faculty of Electrical and Computer Engineering, University Akli Mohand Oulhadj, Rue Drissi Yahia, 10000 Bouira, Algeria
[*] Corresponding author, e-mail: nadia.radja@ummto.dz

Received: 27 January 2025, Accepted: 12 August 2025, Published online: 22 September 2025

Abstract

Various types of faults can occur in a Permanent Magnet Synchronous Machine (PMSM) system, including bearing faults, electrical short/open circuits, eccentricity faults, and demagnetization faults (DFs). A DF occurs when the magnetic strength of the PMSM's permanent magnets weakens, resulting in reduced output torque, which is undesirable in electric vehicles (EVs). This fault can be attributed to physical damage, high-temperature stress, reverse magnetic fields, and aging. Motor current signature snalysis (MCSA) is a traditional method for detecting motor faults, relying on the extraction of signal features from the stator current. In this study, a simulation model of the PMSM was developed to represent both partial and uniform DFs, allowing for the simulation of varying degrees of demagnetization. Harmonic analysis using fast Fourier transform (FFT) demonstrated that the fault diagnosis method based on harmonic wave analysis is effective only for partial DFs in PMSMs, and not applicable to uniform DFs.

Keywords

permanent magnet synchronous motors, fault diagnosis, demagnetization, motor signature current analysis

1 Introduction

The permanent magnet synchronous motors (MSAPs) are highly recommended in the industry. This is because they have higher efficiency, high output power to volume ratio, high torque to current ratio, etc. [1]. However, since the motor is working in the industrial environment with different stresses, affected by the power supply and load conditions, various faults will inevitably occur in the motor during the course of long-term continuous operation. These faults can seriously affect the reliability and safety of the motor operation, if they cannot be diagnosed and corrected in time, it may cause serious equipment and property damage [2]. Therefore, it is especially important to study the fault detection and diagnosis technology of Permanent Magnet Synchronous Machine (PMSM) [3].

Faults in PMSMs are classified into three parts: electrical such as stator windings short circuits, magnetic such as demagnetization, and mechanical faults such as rotor eccentricities and bearing damages [4]. Demagnetization faults (DFs) in PMSMs generally occur due to several factors such as load situations that require high starting torques and fixture reaction that occurs during the rapid change from transient situation to stationary state, magnetic fields in opposite directions that are caused by currents passing through stator coils in static state and high temperature that occur during winding faults [5].

Demagnetization can be complete, or partial. Partial demagnetization can be symmetric or asymmetric too. Depending on the severity of fault, demagnetization can be reversible or irreversible. However, it has been verified that irreversible demagnetization does not arise in the PMs under the steady states. Instead, it arises under transient states [6].

Therefore, it is very important to diagnose the DF. In recent years, several approaches have been proposed for PMSM fault diagnosis, such as motor current signature analysis (MCSA) [7], zero-sequence voltage component [8], vibration analysis (VA) [9], back electromotive force (back-EMF) and magnetic signals [10]. The magnetic signal is the most direct signal to reveal the DF, but it is difficult to obtain because of the closed characteristic of the motor. Researchers used magnetic leakage as a DF diagnosis signal [11]. Though,

Cite this article as: Radja, N., Yassa, N., Rachek, M., Houassine, H. "Modeling and Detecting the Demagnetization Fault in the Permanent Magnet Synchronous Machine Using the Current Signature Analysis", Periodica Polytechnica Electrical Engineering and Computer Science, 69(4), pp. 372–378, 2025. https://doi.org/10.3311/PPee.40008

the magnetic leakage signal is weak, necessity high precision of the sensor, and therefore an increase the manufacturing costs. In order to reduce the cost, DF diagnosis using stator current signal analysis is also popular because it does not require the installation of additional sensors. The popular, reliable, and very frequently methods used for extracting fault features contain fast Fourier transform (FFT) [12], continuous wavelet transform (CWT), discrete wavelet transform (DWT) [13], S-transform [14], Teager–Kaiser energy operator (TKEO) [15] and Hilbert–Huang transform (HHT) [16]. In addition, there is another method of equivalent network, which use air-gap permeance network as Permanent Magnet (PM) equivalent of magnet synchronous motor in order to online diagnose PM DF through measurement of the flux [17].

The aim of this paper is the modeling of the PMSM under the partial demagnetization with the magnetically coupled electrical circuit (MCEC). The study of the behavior of an electric motor is a difficult task and requires above all a good knowledge of its dynamic model in order to correctly predict, by means of simulation, its behavior in the different modes of operation considered. However, the objectives of a simulation model are different, which has motivated researchers to develop models generally based on the following calculation approaches: MCEC method; reluctance networks method (RNM); finite element method (FEM). These methods are widely detailed in the scientific literature, and present different degrees of complexity. In the field of diagnosis of electrical machines, the FEM is used in order to understand and quantify the local consequences of a fault on the different parts of the machine [18].

For example, the FEM allows the study of the local effects of the failure of breaking bars of the rotor cage in an asynchronous machine, namely excessive local heating due to the increase in currents circulating in the neighboring bars and a strong electro-dynamic stress on these same neighboring bars which can lead to the propagation of the fault. The fundamental principle of this method lies in the division of the field of study into elementary domains of finite dimension. On each domain called finite element, the potential is approximated by a low degree polynomial [19].

The permeance network method is based on the analogy between the magnetic and the electric. This approach makes it possible to take into account the characteristics of the iron used for the construction of the machine. Indeed, the calculation of the different reluctances can only be done by fixing a precise value for the relative reluctance of the iron Riron. The rotational movement of the machine is taken into account by means of variable air gap permeance according to the angular position of the rotor [20]. The MCEC modeling approach is based on analytical modeling. This modeling method is quite generic in the sense that it relies on a description of the electromagnetic couplings within the machine based on the geometric and constitutive topology of the machine. This approach has already been proven for the modeling of asynchronous squirrel cage machines. It has also been adapted to the synchronous machine with PMs and offers a compromise in terms of model precision and computation time. This type of modeling makes it possible to take into account a certain number of faults of electromagnetic origin such as short-circuit faults between stator turns, faults of the rotor bar rupture type and/or short-ring circuit [21].

2 PMSM simulation model establishment under normal and demagnetization condition

2.1 PMSM modeling in abc-phase frame

PMSM are brushless machines with sinusoidal distributed stator windings. The excitation flux of PMSM is produced by the PM rotor and Kirchhoff's law is used to develop the electric model of the PMSM seen in Fig. 1. The magnetic permeability of iron is considered to be infinite; the operation is far from magnetic saturation; the magnetic motive force and the flux profiles are considered sinusoid ally distributed and higher harmonics are neglected. These assumptions are commonly acknowledged as appropriate for a lumped parameter model of the electric motors, as found in the electric motor references *b*. Fig. 1 is a schematic illustration of a three-phase two-pole PMSM.

In Fig. 1, symbols $\boldsymbol{V}_{abc}^{S}$ and $\boldsymbol{i}_{abc}^{S}$ represent terminal voltages and currents in each phase; $\boldsymbol{R}_{abc}^{S}$ and $\boldsymbol{L}_{abc}^{S}$ represent

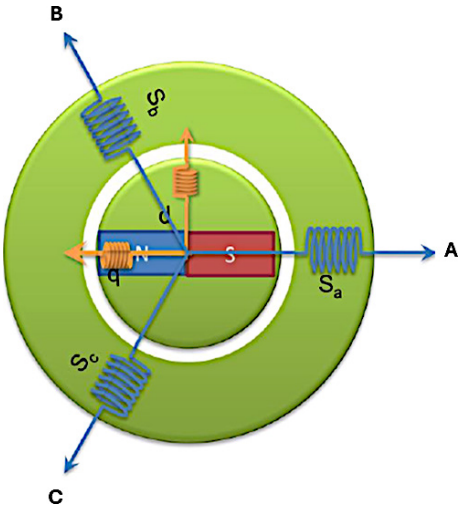

Fig. 1 A two pole PMSM

the stator resistance and inductance respectively, N_s is the turn numbers of each stator winding. Without magnetic saturation, the electrical model of the three-phase PMSM is obtained in its *abc*-phase frame as Eq. (1):

$$\left[\boldsymbol{V}_{abc}^{S}\right]=\left[\boldsymbol{R}_{abc}^{S}\right]\cdot\left[\boldsymbol{i}_{abc}^{S}\right]+\frac{d\left[\boldsymbol{\varphi}_{abc}^{S}\right]}{dt}, \tag{1}$$

where $\boldsymbol{\varphi}_{abc}^{S}$ denotes stator magnetic fluxes for the three phases. For conciseness, matrix expressions are used to denote three-phase variables, i.e.,:

$$\left[\boldsymbol{V}_{abc}^{S}\right]=\left[\boldsymbol{V}_{a}^{S}\quad\boldsymbol{V}_{b}^{S}\quad\boldsymbol{V}_{c}^{S}\right]^{T}, \tag{2}$$

$$\left[\boldsymbol{R}_{abc}^{S}\right]=\begin{bmatrix}\boldsymbol{R}_{a}^{S}&0&0\\0&\boldsymbol{R}_{b}^{S}&0\\0&0&\boldsymbol{R}_{c}^{S}\end{bmatrix}, \tag{3}$$

$$\left[\boldsymbol{i}_{abc}^{S}\right]=\left[\boldsymbol{i}_{a}^{S}\quad\boldsymbol{i}_{b}^{S}\quad\boldsymbol{i}_{c}^{S}\right]^{T}, \tag{4}$$

$$\left[\boldsymbol{\varphi}_{abc}^{S}\right]=\left[\boldsymbol{\varphi}_{a}^{S}\quad\boldsymbol{\varphi}_{b}^{S}\quad\boldsymbol{\varphi}_{c}^{S}\right], \tag{5}$$

Equation (1) is based on the magnetic circuit of the motor in Fig. 1. The stator phase voltages are composed of two parts: a resistive part representing the voltage drops across the stator resistance, and a magnetic part resulting from the changing of the stator magnetic flux linkage. This model generally applies to PMSMs with both symmetrical and asymmetrical phase windings. The winding asymmetry can be represented by variations in resistances matrix and inductances related to the magnetic flux.

Thus, $\boldsymbol{\varphi}_{abc}^{S}$ can be calculated according to Eq. (6):

$$\left[\boldsymbol{\varphi}_{abc}^{S}\right]=\left[\boldsymbol{L}_{abc}^{S}\right]\cdot\left[\boldsymbol{i}_{abc}^{S}\right]+\left[\boldsymbol{\varphi}_{mabc}\right]. \tag{6}$$

Stator inductance $\boldsymbol{L}_{abc}^{S}$ is a (3 × 3) symmetric matrix as defined in Eq. (7). The diagonal elements are the self-inductances of each winding, and the off diagonal elements are the mutual inductances between different phase windings.

$$\left[\boldsymbol{L}_{abc}^{S}\right]=\begin{bmatrix}\boldsymbol{L}_{a}^{S}&\boldsymbol{L}_{ab}&\boldsymbol{L}_{ac}\\\boldsymbol{L}_{ba}&\boldsymbol{L}_{b}^{S}&\boldsymbol{L}_{bc}\\\boldsymbol{L}_{ca}&\boldsymbol{L}_{bc}&\boldsymbol{L}_{c}^{S}\end{bmatrix} \tag{7}$$

The flux linkage generated by PM $\boldsymbol{\varphi}_{mabc}$ relates to the rotor electrical angular position θ_r.

Assuming that the stator windings are placed evenly with a relative phase angle of 120° and the flux linkage distribution obeys the sinusoidal law, $\boldsymbol{\varphi}_{mabc}$ can then be expressed as periodic functions of θ_r defined by Eq. (8):

$$\left[\boldsymbol{\varphi}_{mabc}\right]=\left[\boldsymbol{\varphi}_{ma}\left(\theta_r\right)\quad\boldsymbol{\varphi}_{mb}\left(\theta_r\right)\quad\boldsymbol{\varphi}_{mc}\left(\theta_r\right)\right]^{T}, \tag{8}$$

where φ_m is the magnitude of the PM flux linkage.

$$\left[\boldsymbol{\varphi}_{mabc}\right]=\varphi_m\left[\sin\left(\theta_r\right)\quad\sin\left(\theta_r-\frac{2\pi}{3}\right)\quad\sin\left(\theta_r+\frac{2\pi}{3}\right)\right]^{T} \tag{9}$$

Now, voltage Eq. (1) can be rewritten as Eq. (12) using Eqs. (1) and (2):

$$\left[\boldsymbol{V}_{abc}^{S}\right]=\left[\boldsymbol{R}_{abc}^{S}\right]\cdot\left[\boldsymbol{i}_{abc}^{S}\right]+\frac{d\left[\boldsymbol{L}_{abc}^{S}\right]\cdot\left[\boldsymbol{i}_{abc}^{S}\right]}{dt}+\frac{d\left[\boldsymbol{\varphi}_{mabc}\right]}{dt}, \tag{10}$$

$$\begin{aligned}\left[\boldsymbol{V}_{abc}^{S}\right]&=\left[\boldsymbol{R}_{abc}^{S}\right]\cdot\left[\boldsymbol{i}_{abc}^{S}\right]+\frac{d\theta_r}{dt}\frac{d\left[\boldsymbol{L}_{abc}^{S}\right]}{d\theta_r}\left[\boldsymbol{i}_{abc}^{S}\right]\\&+\left[\boldsymbol{L}_{abc}^{S}\right]\cdot\frac{d\left[\boldsymbol{i}_{abc}^{S}\right]}{dt}+\frac{d\theta_r}{dt}\cdot\frac{d\left[\boldsymbol{\varphi}_{mabc}\right]}{d\theta_r},\end{aligned} \tag{11}$$

$$\begin{aligned}\left[\boldsymbol{V}_{abc}^{S}\right]&=\left[\boldsymbol{R}_{abc}^{S}\right]\cdot\left[\boldsymbol{i}_{abc}^{S}\right]+\omega_r\cdot\frac{d\left[\boldsymbol{L}_{abc}^{S}\right]}{d\theta_r}\left[\boldsymbol{i}_{abc}^{S}\right]\\&+\left[\boldsymbol{L}_{abc}^{S}\right]\cdot\frac{d\left[\boldsymbol{i}_{abc}^{S}\right]}{dt}+\omega_r\cdot\frac{d\left[\boldsymbol{\varphi}_{mabc}\right]}{d\theta_r},\end{aligned} \tag{12}$$

where:

$$\begin{aligned}&\frac{d\left[\boldsymbol{\varphi}_{mabc}\right]}{d\theta_r}\\&=\varphi_m\left[\cos\left(\theta_r\right)\quad\cos\left(\theta_r-\frac{2\pi}{3}\right)\quad\cos\left(\theta_r+\frac{2\pi}{3}\right)\right]^{T}.\end{aligned} \tag{13}$$

In Eq. (12), the rotor angle θ_r and the electrical angular velocity ω_r are two unknown variables that need to be calculated before solving the equation. To do this PMSM's mechanical dynamic equations are incorporated. The mechanical model can be described using Eqs. (14) and (15):

$$\frac{d\omega_r}{dt}=\frac{1}{J}n_p\left[T_e-B_m\frac{\omega_r}{n_p}-T_l\right], \tag{14}$$

$$\frac{d\theta_r}{dt}=\omega_r, \tag{15}$$

where n_p is the number of the pole pairs of the motor, J is the inertia of the rotor, B_m is the viscous friction coefficient. T_e is the electromagnetic torque and T_l is the load torque of the motor. The electromagnetic torque T_e generated by PMSM can be derived from the co-energy W_c of the magnetic system as given in Eq. (16):

$$T_e=n_p\frac{dW_c}{d\theta_r}, \tag{16}$$

with:

$$W_c=\frac{1}{2}\left[\boldsymbol{i}_{abc}^{S}\right]^{T}\left[\boldsymbol{L}_{abc}^{S}\right]\left[\boldsymbol{i}_{abc}^{S}\right]+\left[\boldsymbol{i}_{abc}^{S}\right]^{T}\left[\boldsymbol{\varphi}_{mabc}\right]. \tag{17}$$

The torque can be expressed using phase currents and rotor angular position as in Eq. (18):

$$T_e = n_p\left(\frac{1}{2}\left[\boldsymbol{i}_{abc}^{S}\right]^T\frac{d\left[\boldsymbol{L}_{abc}^{S}\right]}{d\theta_r}\left[\boldsymbol{i}_{abc}^{S}\right]+\left[\boldsymbol{i}_{abc}^{S}\right]^T\frac{d\left[\boldsymbol{\varphi}_{mabc}\right]}{d\theta_r}\right). \quad (18)$$

T_e can be rewritten as follows:

$$T_e = n_p\left(\left[T_S\right]^T\left[\boldsymbol{i}_{abc}^{S}\right]+\left[T_m\right]\right), \quad (19)$$

where:

$$\left[\boldsymbol{T}_S\right] = \frac{1}{2}\left[\boldsymbol{i}_{abc}^{S}\right]^T\frac{d\left[\boldsymbol{L}_{abc}^{S}\right]}{d\theta_r}, \quad (20)$$

$$T_m = \left[\boldsymbol{i}_{abc}^{S}\right]^T\frac{d\left[\boldsymbol{\varphi}_{mabc}\right]}{d\theta_r}. \quad (21)$$

Introducing the electromagnetic expression Eq. (19) in the mechanical Eq. (14), we obtain:

$$T_m - T_l = \frac{J}{n_p}\frac{d\omega_r}{dt} - \left[\boldsymbol{T}_S\right]^T\left[\boldsymbol{i}_{abc}^{S}\right] + B_m\omega_r. \quad (22)$$

Hence the PMSM space state model is given by:

$$\begin{bmatrix}\left[\boldsymbol{V}_{abc}^{S}\right]\\ T_m - T_l\\ 0\end{bmatrix} = \begin{bmatrix}\left(\left[\boldsymbol{R}_{abc}^{S}\right]+\omega_r\cdot\frac{d\left[\boldsymbol{L}_{abc}^{S}\right]}{d\theta_r}\right) & \frac{d\left[\boldsymbol{\varphi}_{mabc}\right]}{d\theta_r} & 0\\ -\left[\boldsymbol{T}_S\right] & B_m & 0\\ 0 & -1 & 0\end{bmatrix}\begin{bmatrix}\left[\boldsymbol{i}_{abc}^{S}\right]\\ \omega_r\\ \theta_r\end{bmatrix} + \begin{bmatrix}\left[\boldsymbol{L}_{abc}^{S}\right] & 0 & 0\\ [0] & \frac{J}{n_p} & 0\\ 0 & 0 & 1\end{bmatrix}\cdot\frac{d}{dt}\begin{bmatrix}\left[\boldsymbol{i}_{abc}^{S}\right]\\ \omega_r\\ \boldsymbol{\theta}_r\end{bmatrix}. \quad (23)$$

The differential equations system (Eq. (23)) is solved using the fourth order Rung–Kutta method while the step time is chosen at each time as the inverse of the maximal eigen values of the state matrix.

2.2 Analysis of the PMSM partial DF performance

PMSM DF can be divided into two kinds. One is entire PM poles occurrence uniform demagnetization to a certain extent, which is called whole demagnetization or uniform demagnetization, and the second is partial PM poles occurrence demagnetization to a certain extent, which is called partial demagnetization or local partial [8].

In the case of DF, the flux (φ_{rdem}) of the demagnetized magnets in Eq. (24) will change according to the severity and the position of the demagnetized magnets is determined using Eq. (24):

$$\varphi_{rdem} = \varphi_r\left(1-\varphi_{rdemag}\right), \quad (24)$$

where φ_{rdemag} is the percentage of demagnetization.

And the linkage flux can be rewritten in Eqs. (25) and (26):

$$\left[\boldsymbol{\varphi}_{demabc}\right] = \left[\boldsymbol{\varphi}_{rdema}\left(\theta_r\right)\quad\boldsymbol{\varphi}_{rdemb}\left(\theta_r\right)\quad\boldsymbol{\varphi}_{rdemc}\left(\theta_r\right)\right]^T, \quad (25)$$

$$\left[\boldsymbol{\varphi}_{demabc}\right] = \begin{bmatrix}\varphi_{rdem}\cdot\sin\left(\theta_r\right)\\ \varphi_{rdem}\cdot\sin\left(\theta_r-\frac{2\pi}{3}\right)\\ \varphi_{rdem}\cdot\sin\left(\theta_r+\frac{2\pi}{3}\right)\end{bmatrix}. \quad (26)$$

In the presence of the DF, the PMSM space state model is given by:

$$\begin{bmatrix}\left[\boldsymbol{V}_{abc}^{S}\right]\\ T_m - T_l\\ 0\end{bmatrix} = \begin{bmatrix}\left(\left[\boldsymbol{R}_{abc}^{S}\right]+\omega_r\cdot\frac{d\left[\boldsymbol{L}_{abc}^{S}\right]}{d\theta_r}\right) & \frac{d\left[\boldsymbol{\varphi}_{demabc}\right]}{d\theta_r} & 0\\ -\left[\boldsymbol{T}_S\right]^T & B_m & 0\\ 0 & -1 & 0\end{bmatrix}\begin{bmatrix}\left[\boldsymbol{i}_{abc}^{S}\right]\\ \omega_r\\ \theta_r\end{bmatrix} + \begin{bmatrix}\left[\boldsymbol{L}_{abc}^{S}\right] & 0 & 0\\ [0] & \frac{J}{n_p} & 0\\ 0 & 0 & 1\end{bmatrix}\cdot\frac{d}{dt}\begin{bmatrix}\left[\boldsymbol{i}_{abc}^{S}\right]\\ \omega_r\\ \theta_r\end{bmatrix}, \quad (27)$$

where:

$$T_m = \left[\boldsymbol{i}_{abc}^{S}\right]^T\frac{d\left[\boldsymbol{\varphi}_{demabc}\right]}{d\theta_r}, \quad (28)$$

and:

$$\left[\boldsymbol{\varphi}_{abc}^{S}\right] = \left[\boldsymbol{L}_{abc}^{S}\right]\cdot\left[\boldsymbol{i}_{abc}^{S}\right] + \left[\boldsymbol{\varphi}_{demabc}\right]. \quad (29)$$

3 Simulation results and discussions

The simulation parameters of the PMSM are given in Table 1.

Applying the sinusoidal AC voltage source, setting the resistance and reactance parameters, a simulation model was established. The simulation flux linkage wave form, the electromotive force and the stator currents under the

Table 1 Specification on the presented PMSM

Components	Rating values
Rated power (P_n)	335 W
Voltage (V)	32.5
Frequency (f)	50 Hz
Rated speed (N_n)	1000 rpm
Number of poles pairs (n_p)	3
Stator resistance (R_s)	1 Ohm
Inductance ($L_s = L_{ls} + L_m$)	3.2 mH
Mutual inductance (L_m)	0.13 mH
Magnetic flux (φ_m)	0.3 Web
Moment of inertia (J)	0.00065 kg m^2

PM of normal, 5% partial demagnetization, 10% partial demagnetization and 15% partial demagnetization at the speed of 1000 rmp are shown in Figs. 2 to 10.

It can be seen that the phase current, the electromotive force and the flux are unbalanced during demagnetization. Meanwhile, the harmonics component increase. Thus, it is very important to monitor the PM flux variation during motor operation and then detect the demagnetization in its early stage to maintain the healthy motor operating.

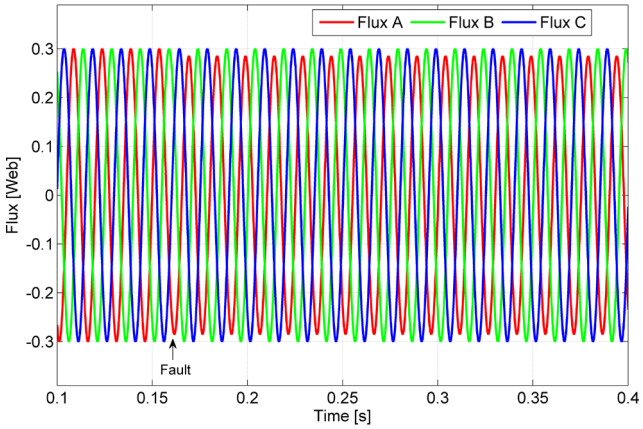

Fig. 2 Flux linkage under 5% of the asymmetric demagnetization

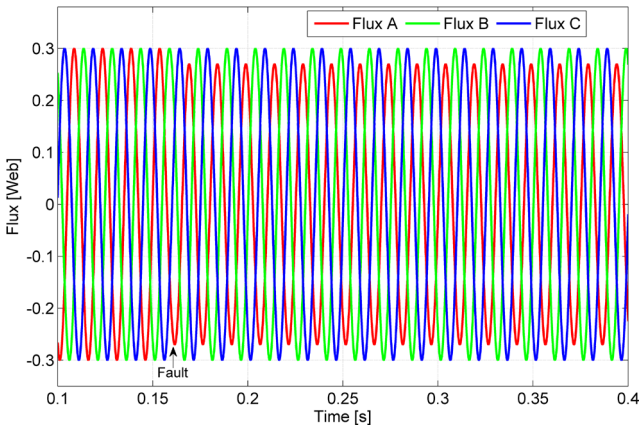

Fig. 3 Flux linkage under 10% of the asymmetric demagnetization

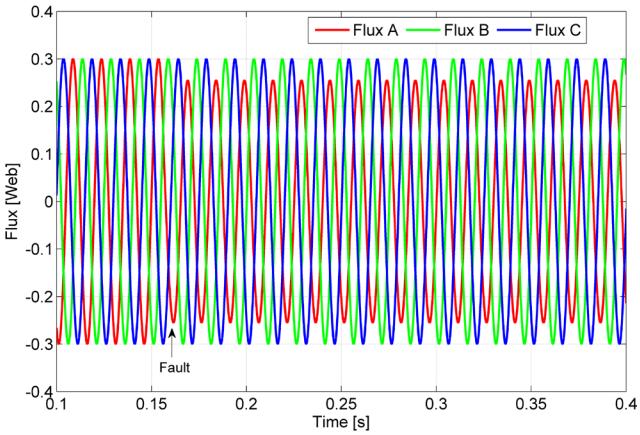

Fig. 4 Flux linkage under 15% of the asymmetric demagnetization

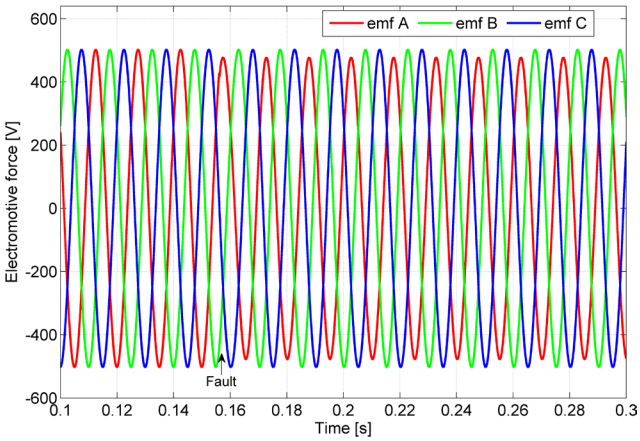

Fig. 5 Electromotive force under 5% of the asymmetric demagnetization

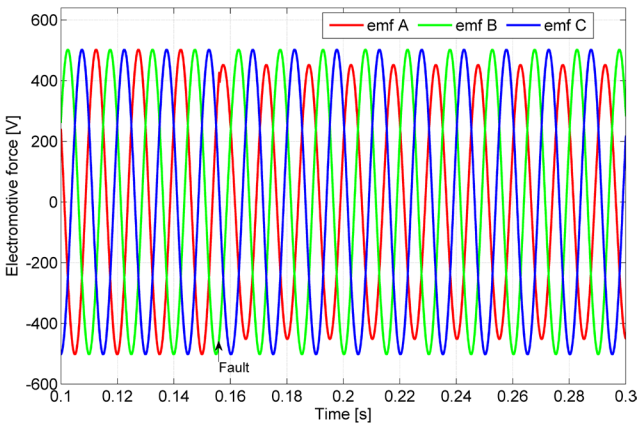

Fig. 6 Electromotive force under 10% of the asymmetric demagnetization

When DF occur in the rotor of the PMSM, the flux linkage fundamental wave amplitude significantly reduces relative to the rotor normal condition, and when the increase of rotor demagnetization degree the fundamental wave amplitude gets smaller and smaller [8].

Current based detection approach is popular due to the easy availability of the current signal, and simple mathematical model. Researchers are trying to use current frequency distribution, harmonic component and injected

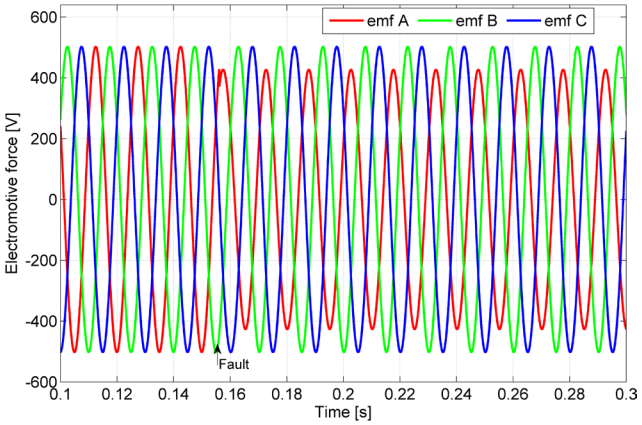

Fig. 7 Electromotive force under 15% of the asymmetric demagnetization

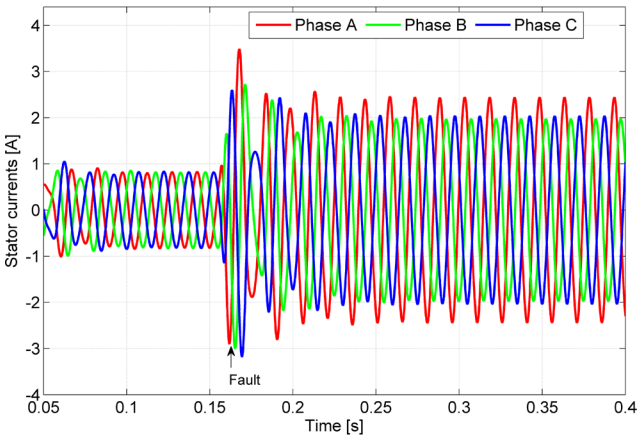

Fig. 8 Temporal evolution of the phase currents in case of 5% of the asymmetric demagnetization

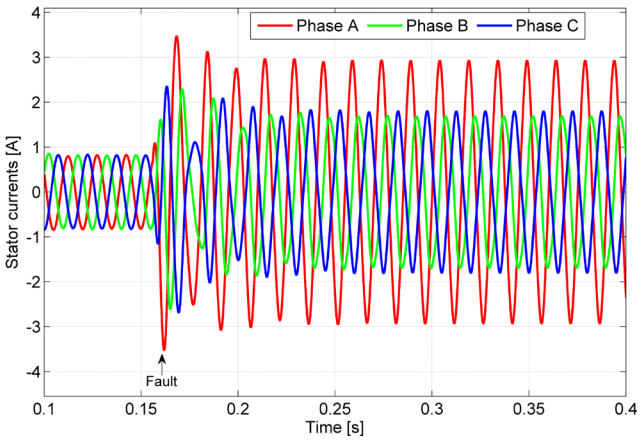

Fig. 9 Temporal evolution of the phase currents in case of 10% of the asymmetric demagnetization

current to detect the PM filed fault. Stator phase currents frequency distribution is used to describe the fault distribution by FFT averages in time domain, but it is not applicable to variable speed and load because frequency components appearing asymmetrical stator windings gives improper fault analysis result.

Figs. 11 to 13 show the power spectral density under different percentages of asymmetric demagnetization.

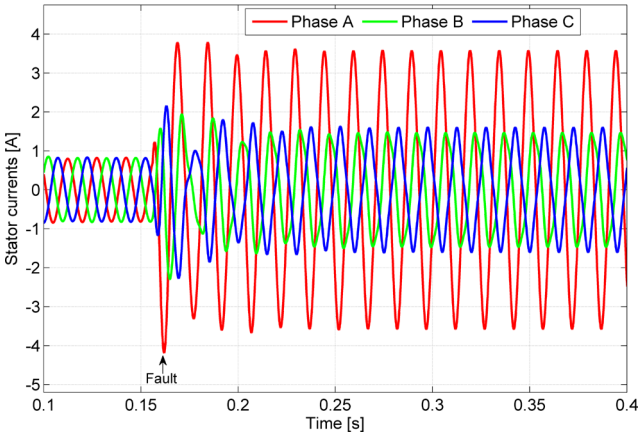

Fig. 10 Temporal evolution of the phase currents in case of 15% of the asymmetric demagnetization

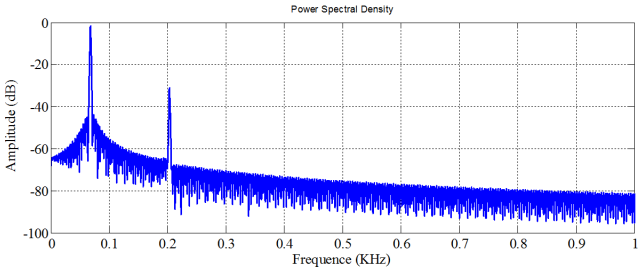

Fig. 11 Power spectral density under 5% of the asymmetric demagnetization

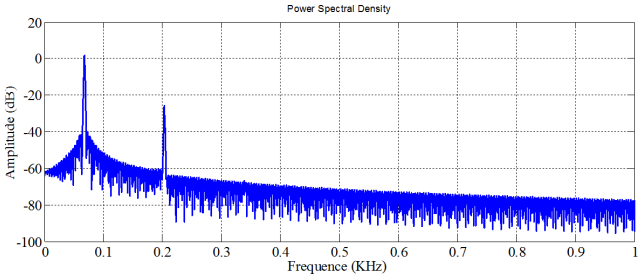

Fig. 12 Power spectral density under 10% of the asymmetric demagnetization

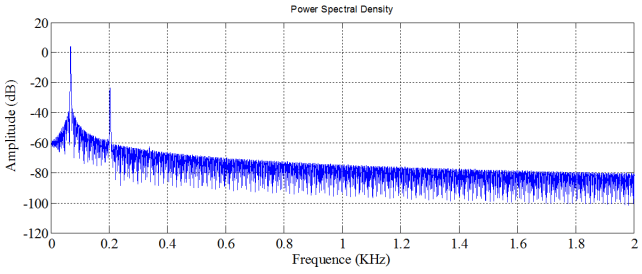

Fig. 13 Power spectral density under 15% of the asymmetric demagnetization

4 Conclusion

Partial DF of the PMSM in varying degrees under load state have been simulated using analysis software. In this paper, the simulation results show that the reasonable DF waveform can be obtained by changing the PM material parameters, and the partial demagnetization simulations

show that the magnetic field strength will be reduced with the increase of DF severity. The harmonic analysis shows that the harmonic amplitude is increased significantly under the partial DF condition.

References

[1] Ji, W., Ni, F., Gao, D., Luo, S., Lv, Q., Lv, D. "Electromagnetic Design of High-Power and High-Speed Permanent Magnet Synchronous Motor Considering Loss Characteristics", Energies, 14(12), 3622, 2021. https://doi.org/10.3390/en14123622

[2] Chen, Y., Liang, S., Li, W., Liang, H., Wang, C. "Faults and Diagnosis Methods of Permanent Magnet Synchronous Motors: A Review", Applied Sciences, 9(10), 2116, 2019. https://doi.org/10.3390/app9102116

[3] Wang, Z., Song, Y., Sun, F., Cao, C. "Research on Fault Detection and Diagnosis of Stator Windings in Permanent Magnet Synchronous Motor", In: International Conference on Energy, Ecology and Environment (ICEEE 2018), Melbourne, Australia, 2018. ISBN 978-1-60595-590-2 https://doi.org/10.12783/dteees/iceee2018/27846

[4] Wang, Z., Yang, J., Ye, H., Zhou, W. "A review of Permanent Magnet Synchronous Motor fault diagnosis", In: 2014 IEEE Conference and Expo Transportation Electrification Asia-Pacific (ITEC Asia-Pacific), Beijing, China, 2014, pp. 1–5. ISBN 978-1-4799-4239-8 http://doi.org/10.1109/ITEC-AP.2014.6940870

[5] Akar, M., Eker, M. "Demagnetization Fault Diagnosis in Permanent Magnet Synchronous Motors", Przegląd Elektrotechniczny, 89(2), pp. 229–233, 2013. [online] Available at: https://pe.org.pl/articles/2013/2a/49.pdf [Accessed: 26 January 2025]

[6] Ebrahim, B. M., Faiz, J. "Demagnetization Fault Diagnosis in Surface Mounted Permanent Magnet Synchronous Motors", IEEE Transactions on Magnetics, 49(3), pp. 1185–1192, 2013. http://doi.org/10.1109/TMAG.2012.2217978

[7] Badawy, M. A. E., Mohamed, M. M. A., Saad, A. A. A. "Diagnosis of the Electric Vehicles Synchronous Motors Faults Using Signal Analysis Techniques", Engineering Research Journal, 182(2), pp. 195–208, 2024. http://doi.org/10.21608/erj.2024.358547

[8] Urresty, J.-C., Riba, J.-R., Delgado, M., Romeral, L. "Detection of Demagnetization Faults in Surface-Mounted Permanent Magnet Synchronous Motors by Means of the Zero-Sequence Voltage Component", IEEE Transactions on Energy Conversion, 27(1), pp. 42–51, 2012. http://doi.org/10.1109/TEC.2011.2176127

[9] Ogidi, O. O., Barendse, P. S., Khan, M. A. "Detection of Static Eccentricities in Axial-Flux Permanent-Magnet Machines With Concentrated Windings Using Vibration Analysis", IEEE Transactions on Industry Applications, 51(6), pp. 4425–4434, 2015. http://doi.org/10.1109/TIA.2015.2448672

[10] Urresty, J.-C., Riba, J.-R., Romeral, L. "A Back-emf Based Method to Detect Magnet Failures in PMSMs", IEEE Transactions on Magnetics, 49(1), pp. 591–598, 2013. http://doi.org/10.1109/TMAG.2012.2207731

[11] Huang, F., Zhang, X., Qin, G., Xie, J., Peng, J., Huang, S., Long, Z., Tang, Y. "Demagnetization Fault Diagnosis of Permanent Magnet Synchronous Motors Using Magnetic Leakage Signals", IEEE Transactions on Industrial Informatics, 19(4), pp. 6105–6116, 2023. http://doi.org/10.1109/TII.2022.3165283

[12] de Jesus Romero-Troncoso, R. "Multirate Signal Processing to Improve FFT-Based Analysis for Detecting Faults in Induction Motors", IEEE Transactions on Industrial Informatics, 13(3), pp. 1291–1300, 2017. http://doi.org/10.1109/TII.2016.2603968

[13] Riba Ruiz, J.-R., Rosero, J. A., Garcia Espinosa, A., Romeral, L. "Detection of Demagnetization Faults in Permanent-Magnet Synchronous Motors Under Nonstationary Conditions", IEEE Transactions on Magnetics, 45(7), pp. 2961–2969, 2009. http://doi.org/10.1109/TMAG.2009.2015942

[14] Song, X., Zhao, J., Song, J., Dong, F., Xu, L. Zhao, J. "Local Demagnetization Fault Recognition of Permanent Magnet Synchronous Linear Motor Based on S-Transform and PSO–LSSVM", IEEE Transactions on Power Electronics, 35(8), pp. 7816–7825, 2020. http://doi.org/10.1109/TPEL.2020.2967053

[15] Song, J., Zhao, J., Zhang, X., Dong, F., Zhao, J., Xu, L., Yao, Z. "Accurate Demagnetization Faults Detection of Dual-Sided Permanent Magnet Linear Motor Using Enveloping and Time-Domain Energy Analysis", IEEE Transactions on Industrial Informatics, 16(10), pp. 6334–6346, 2020. http://doi.org/10.1109/TII.2019.2962730

[16] Guo, Z., Yang, S., Yu, W., Zhang, L., Zhong, Z. Sui, Y. "Non-communication protection scheme for power transmission system based on transient currents, HHT and SVM", IET Generation, Transmission & Distribution, 12(12), pp. 2816–2824, 2018. https://doi.org/10.1049/iet-gtd.2017.0862

[17] Konar, P., Chattopadhyay, P. "Multi-class fault diagnosis of induction motor using Hilbert and Wavelet Transform", Applied Soft Computing, 30, pp. 341–352, 2015. https://doi.org/10.1016/j.asoc.2014.11.062

[18] Zhang, Z., Ma, H., Yang, C., Yuan, D. "Study on Permanent Magnet Synchronous Demagnetization Fault Performance", Sensors & Transducers, 173(6), pp. 82–89, 2014. [online] Available at: https://www.researchgate.net/publication/286190937_Study_on_Permanent_Magnet_Synchronous_Demagnetization_Fault_Performance [Accessed: 26 January 2025]

[19] Usman, A., Joshi, B. M., Rajpurohit, B. S. "Review of fault modeling methods for permanent magnet synchronous motors and their comparison", In: 2017 IEEE 11th International Symposium on Diagnostics for Electrical Machines, Power Electronics and Drives (SDEMPED), Tinos, Greece, 2017, pp. 141–146. ISBN 978-1-5090-0410-2 http://doi.org/10.1109/DEMPED.2017.8062347

[20] Hang, J., Zhang, J., Xia, M., Ding, S., Hua, W. "Interturn Fault Diagnosis for Model-Predictive-Controlled-PMSM Based on Cost Function and Wavelet Transform", IEEE Transactions on Power Electronics, 35(6), pp. 6405–6418, 2020. http://doi.org/10.1109/TPEL.2019.2953269

[21] Hannon, B., Sergeant, P., Dupré, L. Pfister, P.-D. "Two-Dimensional Fourier-Based Modeling of Electric Machines—An Overview", IEEE Transactions on Magnetics, 55(10), 8107217, 2019. http://doi.org/10.1109/TMAG.2019.2923544